

Research Paper

# CPNE8 Promotes Gastric Cancer Metastasis by Modulating Focal Adhesion Pathway and Tumor Microenvironment

Peiling Zhang<sup>1#</sup>, Xiaofei Cao<sup>1#</sup>, Mingmei Guan<sup>1#</sup>, Dailing Li<sup>1</sup>, Hong Xiang<sup>1</sup>, Qian Peng<sup>1</sup>, Yun Zhou<sup>1</sup>, Chengyin Weng<sup>1</sup>, Xisheng Fang<sup>1</sup>, Xia Liu<sup>1</sup>, Haibo Mao<sup>1</sup>, Qiao Li<sup>2✉</sup>, Guolong Liu<sup>1✉</sup>, Lin Lu<sup>1 ✉</sup>

1. Department of Medical Oncology, the Second Affiliated Hospital, School of Medicine, South China University of Technology, Guangzhou, Guangdong, China
2. Department of Surgery University of Michigan, Ann Arbor, Michigan, USA

#Peiling Zhang, Xiaofei Cao and Mingmei Guan contributed equally to this work

✉ Corresponding author: Dr. Lin Lu, [eylinlv@scut.edu.cn](mailto:eylinlv@scut.edu.cn); Dr. Guolong Liu, [eygliu@scut.edu.cn](mailto:eygliu@scut.edu.cn); Dr. Qiao Li, [qiaoli@umich.edu](mailto:qiaoli@umich.edu)

© The author(s). This is an open access article distributed under the terms of the Creative Commons Attribution License (<https://creativecommons.org/licenses/by/4.0/>). See <http://ivyspring.com/terms> for full terms and conditions.

Received: 2022.06.22; Accepted: 2022.07.13; Published: 2022.07.25

## Abstract

Little is known about the oncogenic role or biological function of copine VIII (CPNE8) in gastric cancer (GC). Based on TCGA database, we screened for CPNE8 and analyzed the expression of CPNE8 in GC. The correlations between CPNE8 and clinical features were analyzed using TCGA and GEO databases. The prognostic value of CPNE8 was assessed using Cox analysis and Kaplan–Meier curves. The results showed that increased expression of CPNE8 was positively correlated with metastasis and can be considered an independent prognostic risk factor for poor survival. We found that CPNE8 can promote cell proliferation, migration, and invasiveness in GC using *in vitro* and *in vivo* experiments. Our study demonstrated that CPNE8 promotes tumor progression via regulation of focal adhesion, and these effects can be rescued by focal adhesion kinase (FAK) inhibitor GSK2256098 or knockdown of FAK. In addition, CPNE8 was correlated significantly with the infiltration of cancer-associated fibroblasts and immune cells, as demonstrated by various algorithms, and high CPNE8 expression predicted poor efficacy of immune checkpoint therapy. Our findings suggest that CPNE8 modulates focal adhesion and tumor microenvironment to promote GC progression and invasiveness and could serve as a novel prognostic biomarker in GC.

Key words: CPNE8; Gastric cancer; Metastasis; Focal adhesion; Tumor microenvironment.

## Introduction

Gastric cancer (GC) ranks fifth in incidence and fourth in mortality worldwide [1]. East Asia is among the regions with a high incidence of GC, and the incidence of GC is highest of all in China [2]. Despite the advanced development of tumor-targeted therapy and immunotherapy, the prognosis of GC patients remains poor, with a 5-year overall survival rate of only approximately 30% [3-5]. GC is highly susceptible to distant metastasis, leading to failure of traditional treatment strategies such as chemotherapy and radiotherapy [6]. In fact, approximately 50–65% of GC patients are diagnosed at an advanced stage with extensive invasive or distant metastases, and

these patients gain limited therapeutic benefit from treatment [7-9]. Therefore, it is important to understand the mechanisms involved in GC progression and metastasis to contribute to the development of improved targeted therapies.

The copine family encodes calcium-dependent phospholipid-binding proteins that may play a role in membrane trafficking and in mediating cellular processes by conferring calcium regulation to various signaling pathways [10, 11]. Increasing evidence has indicated that copine family members are involved in cancer development and progression. Tang summarized the biological properties of the copine

family and their oncogenic roles in several cancers, including breast, colorectal, and non-small cell lung cancers [12]. The copine family of proteins perform different signal transduction functions, such as membrane transport, lipid messenger production, GTPase activation, protein phosphorylation, etc. [13-15]. Studies on the role of CPNEs in cancer are limited, and further research is needed. *CPNE8* (copine VIII), one of the copine family genes, was initially identified as a gene pre-expressed in the prostate and testis. Robust *CPNE8* expression was detected in the prostate, heart, and brain, suggesting that *CPNE8* might play an essential role in the regulation and development of the prostate [16]. CPNE family genes such as *CPNE1* and *CPNE3*, were closely related to tumorigenesis and progression [12, 17, 18]. However, there is limited knowledge regarding the roles and mechanisms of *CPNE8* in carcinogenesis. *CPNE8* could fuse with *AML1* genes to form *AML-CPNE8* chimeras in acute myeloid leukemia (AML) patients, thus negatively regulating the proliferation of AML cancer cells [19]. A recent study suggested that *RP11-396F22.1*, acting as an early diagnostic indicator of cervical cancer, could enhance the progression of cervical cancer by negatively regulating *CPNE8* [20]. Accumulating evidence suggests that *CPNE8* functions in cancer cell migration and invasion. Dang et al. [21] found that *CPNE8* promoted basal-like breast-cancer tumor invasion. Another study showed that *CPNE8* promoted the migration and invasion of pancreatic cancer cells [22].

In this study, we used public databases to investigate the effect of *CPNE8* on GC progression, focusing on GC metastasis. We found that *CPNE8* was indeed a metastasis-related gene. High expression of *CPNE8* in GC patients was closely associated with various clinicopathological features and predicts poor prognostic outcomes. Furthermore, we screened the downstream targets of *CPNE8* and explored their regulatory mechanisms. In addition, *CPNE8* expression is associated with multiple immune cell infiltrations in the tumor microenvironment, which may lead to GC metastasis. These findings provide a novel approach to the diagnosis and treatment of metastatic GC.

## Materials and Methods

### Characteristics of patients and ethical statement

A total of 55 patients with GC were included in this study. The patients met the diagnostic criteria for gastric adenocarcinoma, and none had received any anti-tumor treatment. All human tissues were

obtained after informed consent was obtained. This study was approved by the Research Ethics Committee of the Second Affiliated Hospital of the South China University of Technology, and informed consent was obtained from all patients.

### Data collection and analysis

The mRNA data and clinical data of stomach adenocarcinoma (STAD) patients were downloaded from TCGA database and processed for differentially expressed genes and GSEA (gene-set enrichment analysis) using R scripts. Since various versions of TNM staging were applied to gastric cancer patients in the TCGA-STAD cohort, including the 5th, 6th, and 7th editions. We re-analyzed the clinical data according to the 7th edition of the AJCC TNM staging system and performed it for subsequent analyses. And the modified clinical data was shown in **Table S1**. We used the GSE118916 dataset to analyze the expression of *CPNE8* in GC. Genes associated with *CPNE8* expression were screened for KEGG the Kyoto Encyclopedia of Genes and Genomes (KEGG) and Gene Ontology (GO) for functional enrichment analysis. Statistical significance was set at  $p < 0.05$ .

### Cell culture and transfection

The gastric mucosal epithelial cell line (GES-1) and GC cell lines AGS, BGC823, and MKN45 were obtained from the Global Bioresource Center (ATCC, USA). All cells were cultured in a DMEM medium (Gibco, USA) containing 10% fetal bovine serum (FBS) and 1% penicillin/streptomycin in a humidified atmosphere at 37 °C and 5% CO<sub>2</sub>. The shRNA sequence for *CPNE8* (GAGCATGGCTAGATTGGCTAA, sh-*CPNE8*) was designed and synthesized by IGE Biotechnology (Guangzhou, China). An over-expression plasmid carrying the human *CPNE8* sequence (oe-*CPNE8*) was acquired from Tsingke Biotechnology (Guangzhou, China). Lentiviruses containing scrambled sequences (sh-negative) and an empty vector (oe-vector) were used as controls according to the manufacturer's instructions. GC cells were transfected with lentiviral vectors and then selected with puromycin (a resistance marker) for one week to establish stable cell lines. Transfection efficiency was analyzed by quantitative real-time PCR (qRT-PCR) and Western blotting according to the manufacturer's instructions. We used siRNA targeting *PTK2* (encoding *FAK*) to eliminate *FAK* expression for further rescue experiments. The target sequence of *PTK2* (CCGGTCGAATGATAAGGTGTA, si-*FAK*) was synthesized by Tsingke Biotechnology (Guangzhou, China), and knockdown efficiency was determined by Western blotting.

## Western blot

Whole-cell lysates were prepared by sonication in ice-cold lysis buffer (Beyotime Biotech, Shanghai, China) containing protease inhibitors at 1:100 dilution. Subsequently, total proteins were separated by electrophoresis on 10% SDS-PAGE gels. After electrophoresis, the separated protein bands were transferred to polyvinylidene fluoride (PVDF) membranes (Millipore, Cat. #IPVH00010) and blocked with 5% skim milk for 1 h at room temperature. The membranes were then treated with primary antibodies against *CPNE8* (Cat. #AF9047), *FAK* (cat. #R24277) and *pY397-FAK* (Cat. #381143), total *ERK1/2* (Proteintech, Cat. #67170-1-Ig), phosphorylated *ERK1/2* (Cell Signaling Technology, Cat. # 9101), and *GAPDH* (Cat. # 5174) at a dilution ratio of 1:1000, overnight at 4 °C. The membranes were then washed in TBST for 30 min and incubated with a 1:10 000 HRP-conjugated secondary antibody (Promega, Cat. #W4021; Cat. #W4011) for 1 h at room temperature. The membranes were washed with TBST for 30 min and visualized using ECL kits (Thermo Fisher, Cat. # 34096).

## Quantitative Real-Time PCR

Total RNA was isolated from the cells using TRIzol reagent (Thermo Fisher, Cat. #15596026). Reverse transcription kit (Vazyme, Cat. #R211-01) and ChamQ Universal SYBR qPCR Master Mix (Cat. #Q711) were used for quantitative PCR of the target genes according to the manufacturer's instructions. RT-qPCR primer sequences are listed in **Table S2**. *GAPDH* gene expression was used as the endogenous control. The relative expression of the target genes relative to the control was calculated according to the  $2^{-\Delta\Delta CT}$  formula. Each experiment was performed in triplicate.

## Cell viability assay

Cells were seeded in 96-well plates at a density of  $2 \times 10^3$  cells/well and allowed to grow for 5 days. Each day, 10  $\mu$ l of CCK-8 (Cat. # GK10001-1) was added to 100  $\mu$ l of medium and incubated at 37 °C for 2 h. Absorbance was measured at 450 nm using a multifunctional microplate instrument (Biotek Cytation5, USA). All experiments were performed in triplicate.

## Colony formation

Cells were plated in 6-well plates at a density of 500 AGS cells/well and 250 BGC823 cells/well and allowed to grow for 10 days to form visible colonies. The colonies were fixed with 4% paraformaldehyde for 15 min and stained with 0.1% crystal violet for 20 min at room temperature. The colonies were then

imaged, and the number of colonies counted.

## EDU staining

An EDU staining kit (Beyotime Biotech, Cat. # C0071S) was used for this assay. Stably transfected cells were inoculated at a density of  $5 \times 10^4$  cells/well in a 24-well plate and allowed to adhere overnight for EDU staining. The cells were then washed with PBS and incubated in serum-free DMEM containing 10  $\mu$ M EdU for 2 h. After fixing with 4% paraformaldehyde, the cells were stained to detect proliferating capabilities, according to the manufacturer's instructions. The cells were imaged by fluorescence microscopy, and the percentage of proliferating cells was determined.

## Flow cytometry

For cell cycle assays,  $1 \times 10^6$  cells were washed twice with ice-cold PBS, resuspended in ice-cold 70% ethanol, and fixed overnight at -20 °C. Fixed cells were then centrifuged, resuspended with 0.5 mL/test ( $1 \times 10^6$  cells) PI/RNase Staining Buffer (BD, Cat. #550825), and incubated for 15 min at room temperature before analysis. PE-Annexin V Apoptosis Detection Kit I (Cat. # 559763) was used to detect apoptotic cells, according to the manufacturer's instructions. Flow cytometry was performed using a FACScan instrument (Becton Dickinson, USA), and analysis was performed using FlowJo software.

## Mass spectrometry

Sufficient tumor cells were collected, lysed, and desalted for mass spectrometry analysis. Based on the mass-to-nucleus ratio of different substances, we detected the difference in mass-to-nucleus ratio at the cellular protein level to identify and quantify the differentially expressed proteins. The label-free proteome was detected using a mass spectrometer (Thermo Fisher Orbitrap Plus). Data analysis was performed using the Proteomic Discovery software (ThermoFisher) to obtain data containing Master Protein/Gene, Relative Abundance, GO/KEGG pathway, PSM, and other information for further analysis using bioinformatics methods.

## Wound healing assay

After being imaged at 0 h, cells were cultured in a 37 °C, 5% CO<sub>2</sub> incubator for 24 h and captured under a microscope. Cells were seeded in 24-well plates and cultured to 90% confluence. After 24 h of starvation, the cells were gently scored between monolayers of cultured cells using a sterile 20  $\mu$ l tip and washed twice with PBS. The widths of the original cells and scratches after cell migration were quantified using ImageJ software.

## Migration and invasion assays

Migration and invasion experiments were performed using 24-well Transwell chambers (Cat. #3422) with 8  $\mu\text{m}$  wells. For cell migration experiments,  $0.5 \times 10^5$  cells were resuspended in 200  $\mu\text{l}$  serum-free medium and placed into the upper chambers. Then, 600  $\mu\text{l}$  DMEM containing 10% FBS was added to the lower chambers to incubate the cells for 24 h. For cell invasion experiments, Matrigel (BD, Cat. # 356234) at a dilution of 1:8 was pre-coated on the upper chamber surface, and then  $2 \times 10^5$  cells resuspended in 200  $\mu\text{l}$  serum-free medium were added to the upper chambers. DMEM (600  $\mu\text{l}$ ) containing 10% FBS was added to the lower chambers and incubated for 24–48 h. The cells were then removed from the surface of the upper membrane using a cotton swab and washed three times in PBS to ensure that no cells remained on the surface. The cells were fixed with methanol at room temperature for 15 min and stained with 0.1% crystal violet for 20 min. After washing with PBS, cells were examined and counted under a microscope.

## Cell adhesion assay

The 24-well plates were pre-coated with 10  $\mu\text{g}/\text{ml}$  fibronectin (Cat. # F8180-1ml) overnight at 4  $^{\circ}\text{C}$ , and  $2 \times 10^5$  cells per well were incubated in a 37  $^{\circ}\text{C}$ , 5%  $\text{CO}_2$  incubator for 2 h. The plates were gently washed with PBS to remove the non-adherent cells. Adherent cells were fixed with 4% formaldehyde and stained with 0.1% crystal violet. Cells were imaged and counted under a microscope.

## Select the optimal concentration of FAK inhibitor

GC cells were cultured in a 6-well plate and allowed to reach 70% confluence in regular culture medium. The medium was then replaced with fresh medium containing 0–10  $\mu\text{M}$  GSK2256098 (TargetMol, Cat. #T2281), a small-molecule FAK inhibitor. The cells were incubated for 2 h. At the end of the treatment, the cells were extracted to detect FAK expression levels using western blotting. The concentration with the most significant reduction in FAK protein expression was selected as the optimal concentration for subsequent experiments.

## Animal experiments

All animal experiments were performed according to the protocol approved by the Animal Care and Use Committee of South China University of Technology. Five to 6-week-old male BALB/c nude mice were purchased from Guangdong Scarjindar Biotechnology Co. For the tumor growth model,  $2 \times 10^6$  BGC823-oe-CPNE8 cells and control cells in 200  $\mu\text{l}$

PBS were injected subcutaneously into the left lower dorsum of the nude mice. Tumor volume was measured every 3 days and calculated according to the following formula: tumor volume ( $\text{mm}^3$ ) = length  $\times$  width<sup>2</sup>  $\times$  0.5. BGC823-oe-CPNE8 cells or control cells ( $1 \times 10^6/100 \mu\text{l}$  PBS) were injected into the tail vein of male BALB/c nude mice to induce tumor lung metastasis. After 4 weeks, the mice were sacrificed and all tumors and lungs were surgically removed for imaging and embedding. HE staining was performed to visualize metastatic lesions.

## Immunofluorescence staining

Mouse xenograft tumors were fixed in 4% paraformaldehyde for 24 h, embedded in paraffin, and cut into 5  $\mu\text{m}$  sections. Tissue sections were placed in an oven at 60  $^{\circ}\text{C}$  for 2 h, then routinely dewaxed and heated with sodium citrate buffer (0.01 M, pH 6.0) for antigen repair. After blocking the antigen with goat serum for 30 min, the tissues were incubated with the antibody Ki67 (Zen BioScience, Cat. #381101-50  $\mu\text{l}$ ) overnight at 4  $^{\circ}\text{C}$ . The tissues were stained with secondary antibodies (Cat. # E032620). Parallel staining with secondary antibodies was used as the control for signal specificity. DAPI (Beyotime Biotechnology, Cat. # C1005) was used to stain the nuclei.

## Immunohistochemistry staining

Tissue sections of the xenograft tumors were treated as described above. After antigen repair, endogenous peroxidase was inhibited with 3% hydrogen peroxide for 10 min, blocked with goat serum for 30 min, and incubated with the primary antibody CPNE8 (Proteintech, Cat. #20097-1-AP), FAK (Cat. #R24277) and anti- $\alpha$ -SMA antibodies (Cat. #GB111364), respectively, at a dilution of 1:100, at 4  $^{\circ}\text{C}$  overnight. After washing with PBS, the DAB kit (Cat. #AR1027) was used for immunostaining, and hematoxylin was used for re-staining. The results were analyzed using a microscope. The immunohistochemical score was calculated as the product of the staining intensity (0–3 points) and staining area (0–3 points) by two researchers, ZPL and CXF [23]. The staining intensity was scored as follows: 0 for no staining, 1 point for light yellow, 2 points for yellow, and 3 points for brown. The stained area was scored as follows:  $\leq 5\%$  scored 0, 5–25% scored 1, 25–50% scored 2, and  $\geq 50\%$  scored 3. Immunohistochemistry scores of  $< 3$  indicated a low expression group, and a score  $\geq 3$  indicated a high expression group.

## Immuno-functional analysis

To explore the association of CPNE8 expression with the tumor microenvironment, we evaluated the immune score, estimated score (that implies tumor

purity), and stromal score of GC patients using the R package “estimate” [24]. We visualized the correlation between *CPNE8* expression and cancer-associated fibroblasts (CAFs) using TIMER2 [25]. We also analyzed the relationship between *CPNE8* and CAFs in the GSE84437 database using the R package “estimate.” Using the TISIDB database, we determined the correlation between *CPNE8* and various chemokines and chemokine receptors [26]. IHC and qRT-PCR analyses were performed to verify the relationship between *CPNE8* and CAFs further. We applied the “MCP-counter” algorithm to quantify marker-based gene sets for immune infiltration [27]. We used the R package “GSVA” for single-sample gene set enrichment analysis (ssGSEA), which calculates the absolute enrichment of gene sets in each sample to assess the connection between *CPNE8* and immune-related pathways. We downloaded mutation data from the TCGA-STAD cohort, calculated TMB and MSI scores, and used Spearman’s correlation analysis to characterize their correlation with *CPNE8* expression. Peng et al. designed a new computational framework that integrates two previously studied tumor immune escape mechanisms and tumor immune dysfunction and exclusion (TIDE) scores [28, 29]. We used the TIDE database to calculate the correlation between *CPNE8* and dysfunction and TIDE scores. In addition, we calculated and compared the correlation of *CPNE8* expression with immune checkpoint responses using the chi-squared test.

### Statistical analysis

All statistical analyses were conducted using R software (version 4.0) and GraphPad Prism package (version 8.3). The median of *CPNE8* expression was chosen as the cut-off for the high- and low-expression groups. Student’s t-test or Wilcoxon test was used for comparisons between the two groups. Analysis of variance was used to compare multiple groups. Spearman analysis was used to assess linear relationships. The chi-squared test was used to analyze the correlation between *CPNE8* expression and clinicopathological features or immune responses. For survival analysis, we selected GC patients with detailed survival status and survival time, including all stages of the disease. We used univariate and multivariate analyses to establish Cox regression models and plotted survival curves using the Kaplan–Meier method, including overall survival (OS), progression-free survival (PFS), and disease-free survival (DFS). We also performed ROC analysis using the R package “pROC” to evaluate the performance of multiple genes in the prediction of tumor carcinogenesis and metastasis, as well as survival analysis [30]. All experiments were repeated

at least three times, and the data are expressed as mean  $\pm$  standard deviation (SD). Statistical significance was defined as two-tailed  $p < 0.05$ .

## Results

### CPNE8 expression is increased in GC and associated with poor survival outcomes

To identify candidate genes involved in GC progression and metastasis, we re-analyzed the TCGA stomach adenocarcinoma RNA-seq dataset and screened 16 genes that were highly expressed in GC and associated with metastasis, including *CPNE8* (Figure 1A). Most of these genes were reported to be associated with tumor metastasis, such as *TDO2*, *CYTL1*, and *LDB2*. [31–33]. However, the role of *CPNE8* in GC oncogenesis and metastasis remains poorly understood. Therefore, we analyzed *CPNE8* mRNA levels using publicly available datasets, such as TCGA-STAD and GSE118916 cohorts. In TCGA-STAD data, *CPNE8* was upregulated in GC tissues, compared to normal tissues (Figure 1B,  $p < 0.001$ ). *CPNE8* expression was higher in tumor tissues in the GSE118916 dataset (Figure 1C,  $p < 0.001$ ). Moreover, *CPNE8* expression was upregulated in metastatic GC, compared with that in primary tumors (Figure 1D,  $p < 0.05$ ), especially in patients with liver metastases (Supplementary Figure S1A,  $p < 0.001$ ). These results indicated that *CPNE8* was highly expressed in GC, and metastatic tumors showed higher *CPNE8* expression. To estimate the predictive value of *CPNE8* expression in gastric carcinogenesis and metastasis, we performed ROC analysis on the TCGA-STAD cohort and GSE118916 datasets. CEACAM5, encoding CEA, is usually used as a clinical biomarker for gastrointestinal cancers and may promote tumor development through its role in cell adhesion [34]. The results showed that *CPNE8* was no better a predictor of the carcinogenesis of GC than CEACAM5 (Supplementary Figure S1B, *CPNE8*: AUC=0.5847,  $p = 0.1117$ ; CEACAM5: AUC=0.6351,  $p = 0.0112$ ) in the TCGA-STAD cohort. However, *CPNE8* exhibited excellent performance in the diagnosis of GC compared to CEACAM5 in the GSE118916 dataset (Supplementary Figure S1C, *CPNE8*: AUC=0.9422,  $p < 0.0001$ ; CEACAM5: AUC=0.5911,  $p = 0.3952$ ). Additionally, *CPNE8* exhibited good prediction of metastatic GC (Figure 1E, AUC=0.6439,  $p = 0.0242$ ), supporting the clinical significance of *CPNE8* as an indicator of metastatic GC. Furthermore, the correlations between *CPNE8* expression and GC clinical features were analyzed (Table 1). The data indicated that the expression of *CPNE8* was significantly related to tumor grade ( $p = 0.0212$ ). As shown in Figure 1F, GC patients with advanced-stage

exhibited higher *CPNE8* expression than those in the early stage. Likewise, high *CPNE8* expression was associated with an advanced GC grade (Figure 1G,  $p < 0.05$ ). However, there were no significant relationships between *CPNE8* expression and other clinical features such as sex, tumor invasion depth, and lymph node metastasis (Supplementary Figure S1D-F). These data suggested that high *CPNE8* expression predicts a more malignant phenotype. We further explored the predictive value of *CPNE8* in prognosis and survival of different types of patients. Univariate Cox analysis showed that *CPNE8* expression was a predictor of overall survival in GC patients ( $p < 0.001$ ) and remained an independent factor in multivariate Cox analysis ( $p = 0.009$ ) (Supplementary Figure S2A-B). Kaplan-Meier analysis indicated that higher *CPNE8* expression was significantly associated with worse overall survival (OS), progression-free survival (PFS), and disease-free survival (DFS) ( $p < 0.01$ , Figure 1H-J). ROC curves showed a favorable predictive capacity of *CPNE8* expression for OS, PFS, and DFS in the TCGA-STAD cohort (AUC > 0.5) (Supplementary Figure S2C-E). Immunohistochemistry was used to detect the expression of *CPNE8* in paraffin-embedded GC and normal tissues. Figure 1K shows representative microscopic images of adjacent normal tissue and GC. IHC scores showed that *CPNE8* was upregulated in most GC tissues compared to that in normal tissues ( $p = 0.0198$ , Figure 1L). There was no significant correlation between *CPNE8* expression and TMN stage in our patient samples (data not shown). Survival analysis based on *CPNE8* expression showed that *CPNE8* was significantly associated with poorer overall survival in our patient samples ( $p = 0.0440$ , Figure 1M). Taken together, these data indicate that the *CPNE8* gene was closely related to GC metastasis and is a novel prognostic biomarker that can independently predict a poor outcome in GC patients.

### CPNE8 enhances the proliferation of GC cells

We performed Western blotting to detect the expression levels of *CPNE8* in the three GC cell lines. Our results showed that *CPNE8* was highly expressed in AGS cells and barely detected in BGC823 cells (Figure 2A). To gain insight into the effects of *CPNE8* on the cellular behavior of GC tumorigenesis, we generated the BGC823-oe-*CPNE8* cell line, which stably overexpressed full-length *CPNE8*. We also developed an AGS-sh-*CPNE8* cell line that stably expressed *CPNE8*-shRNA to suppress *CPNE8* expression. The expression levels of *CPNE8* in stably overexpressing or knocked down cell lines were confirmed by Western blot analysis (Figure 2B) and qRT-PCR (Figure 2C). Relative protein expression

(*CPNE8* protein/*GAPDH*) was also quantified and is shown in a column diagram (Figure 2B). To determine the effect of *CPNE8* on cell proliferation, we performed a cell proliferation assay using CCK-8. We found that after stable knockdown of *CPNE8*, the proliferation ability of AGS cells was reduced, while the proliferation ability of BGC823 cells increased with the overexpression of *CPNE8* (Figure 2D). Consistently, knockdown of *CPNE8* significantly attenuated proliferation, whereas overexpression *CPNE8* increased the proliferation of GC cells in colony formation assays (Figure 2E). EDU staining assays also showed significant differences in the proliferative capacities of GC cells with *CPNE8* knockdown or overexpression compared to control cells (Figure 2F). Taken together, these results demonstrate that *CPNE8* promotes GC cell proliferation.

To explore the mechanism of the carcinogenesis-promoting effect of *CPNE8* on GC cells, we performed cell cycle and apoptosis analyses. Flow cytometry analysis showed an increase in the percentage of G1 cells and a decrease in the rate of S/G2 phases in AGS-sh-*CPNE8* cell, while the opposite was observed in BGC823-oe-*CPNE8* cell (Figure 2G). These results indicate that *CPNE8* promoted cellular G1/S phase transition. Knockdown of *CPNE8* increased the percentage of apoptotic cells, although overexpression of *CPNE8* did not significantly affect cell apoptosis (Figure 2H). These results suggested that *CPNE8* is involved in the cell cycle and apoptosis of GC cells.

**Table 1.** Relationship between *CPNE8* expression and clinicopathologic Characteristics of TCGA-STAD patients (n=322)

Characteristics	CPNE8 expression		$\chi^2$	P-value
	Low (n=161)	High (n=161)		
Gender				
Female	61	60	0.01324	0.9084
Male	100	101		
Grade				
G1 + G2	70	50	5.314	0.0212*
G3	91	111		
Invasion depth				
T1 + T2	41	33	1.123	0.2893
T3 + T4	120	128		
Lymph metastasis				
N0 + N1	93	76	3.599	0.0578
N2 + N3	68	85		
Distant metastasis				
M0	154	146	3.122	0.0772
M1	7	15		
TNM stage				
Stage I + II	86	69	3.595	0.058
Stage III + IV	75	92		

\* $p < 0.05$

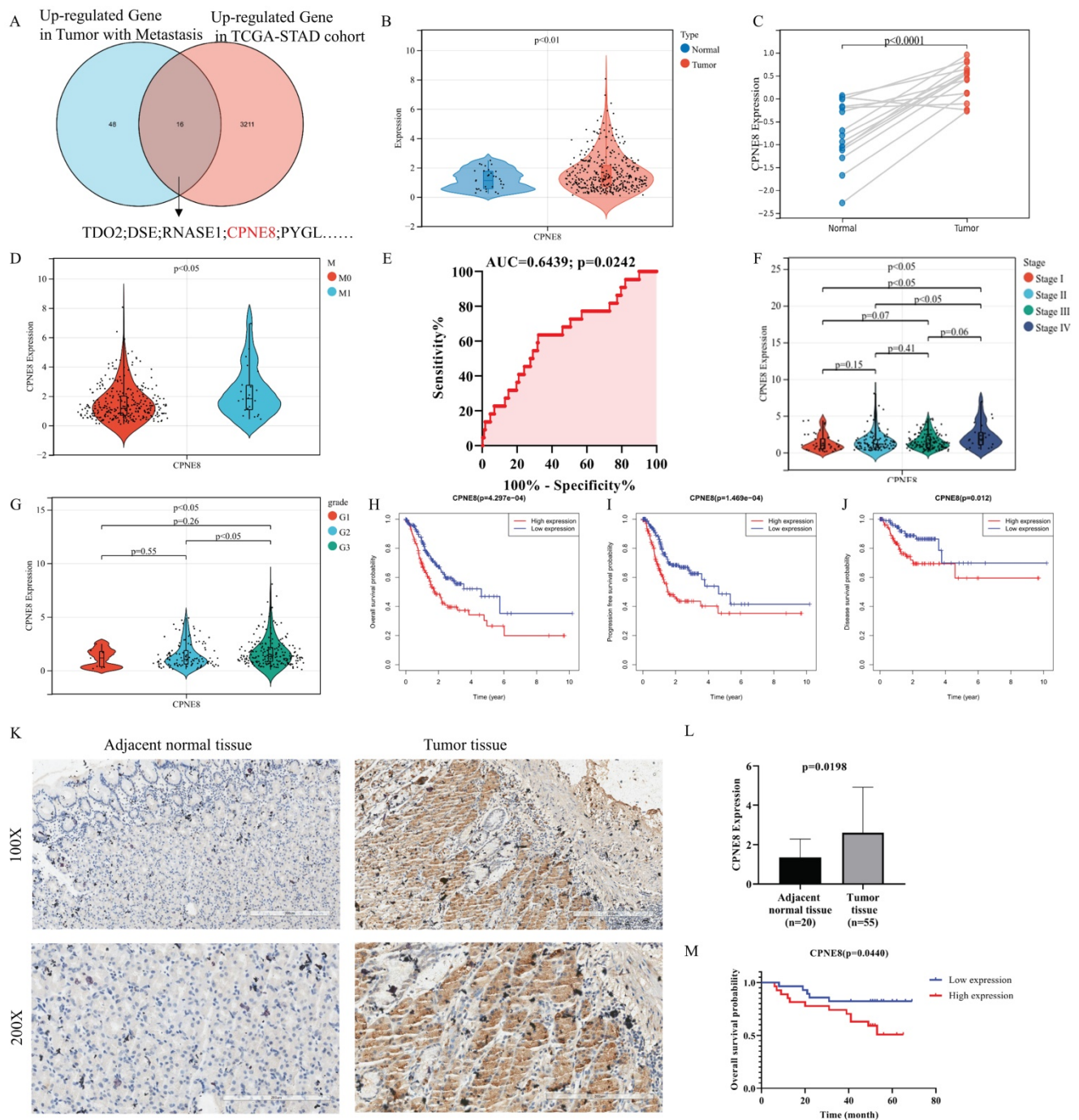


**Figure 1.** *CPNE8* was overexpressed in gastric cancer and associated with poor patient survival. (A) Venn diagram showing genes with high expression and association with tumor metastasis in the TCGA-STAD cohort. (B) Comparison of *CPNE8* gene expression between 375 tumor tissues and 32 normal tissues. (C) Normalized GEO data demonstrating differential expression of *CPNE8* between 15 tumor tissues and paired normal tissues. (D) Increasing *CPNE8* expression in metastatic gastric cancer compared to primary tumors. (E) The area under the ROC curve (AUC) indicated that *CPNE8* revealed better efficiency in predicting metastatic gastric cancer. (F) Significantly different expression of *CPNE8* among tumor stages in the TCGA-STAD cohort. (G) Significantly different expression of *CPNE8* among tumor grades in the TCGA-STAD cohort. (H) Overall survival (OS) curves based on *CPNE8* status. (I) Progression-free survival (PFS) curves based on *CPNE8* expression. (J) Disease-free survival (DFS) curves based on *CPNE8* expression. (K) The representative microscopy images of *CPNE8* in normal tissue and gastric cancer tissue were shown at 100X and 200X magnifications. (L) The IHC scores displayed that *CPNE8* was upregulated in most GC than normal tissue. (M) The overall survival curve was based on *CPNE8* scores obtained by immunohistochemistry.

### CPNE8 promotes GC cell migration and invasion *in vitro*

Considering the significant elevation of *CPNE8* in metastatic GCs, we performed experiments to examine the malignant behavior of invasiveness using wound-healing and Transwell assays. Wound-healing

assays demonstrated that knockdown of *CPNE8* retarded cell migration and motility. By contrast, overexpression of *CPNE8* enhanced cell migration and motility (Figure 3A). Quantitative analysis of wound closure area showed statistically significant differences after knockdown or overexpression of

*CPNE8* compared to controls (**Figure 3B**). Transwell assays showed that migratory and invasive abilities were significantly suppressed after *CPNE8* knockdown, whereas cell migration and invasion capabilities were enhanced using *BGC823-oe-CPNE8* compared with controls (**Figure 3C**). Representative images are shown, and the numbers of migratory and invasive GC cells were quantified in a histogram graph, displaying statistically significant alterations after knockdown or overexpression of *CPNE8* (**Figure 3D**).

Collectively, these results demonstrate that *CPNE8* promotes GC cell migration and invasion *in vitro*.

### **CPNE8 activates the Focal adhesion pathway to promote tumor metastasis**

We investigated the potential mechanism of action of *CPNE8* in GC metastasis. GSEA was performed based on the median expression levels of *CPNE8*, Gene Set Enrichment Analysis (GSEA) was

performed in the TCGA-STAD cohort. A set of signaling pathways, such as focal adhesion, gap junction, and ECM receptor interaction, was functionally enriched in GC patients with high *CPNE8* expression (Supplementary Figure S3A). In addition, we screened genes with strong correlations with *CPNE8* expression ( $|R| \geq 0.4$  and  $p \leq 0.05$ ) using the Cbioportal website for KEGG functional enrichment analysis in the TCGA-STAD cohort. We found that the focal adhesion pathway, cell adhesion molecule (CAMs) pathway, and tight junctions were abundant (Supplementary Figure S3B). These signaling pathways are closely associated with tumor metastasis [35-37]. We performed mass spectrometry analysis on *CPNE8* knockdown cells to screen for differentially expressed proteins for KEGG functional enrichment. Pathway analysis indicated that the genes regulating the focal adhesion pathway were most significantly disrupted after *CPNE8* knockdown (enrichment score = 2.5,  $p < 0.01$ , **Figure 4A**).

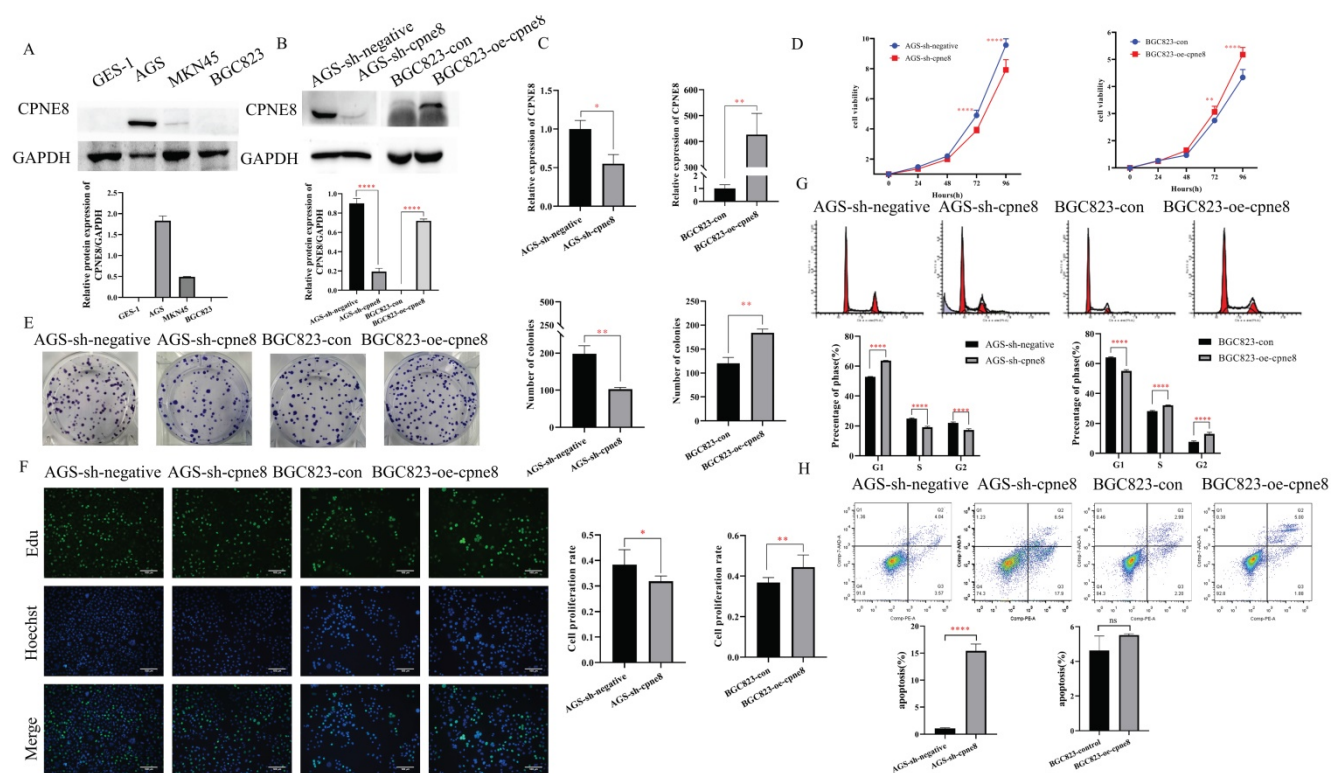


**Figure 2.** *CPNE8* enhanced the proliferation of GC cells. (A) Western blot plots showing the different expressions of the *CPNE8* gene in GC cell lines. Relative protein expression (*CPNE8* protein/GAPDH) was quantified in a column graph. (B) *CPNE8* knockdown and transfection efficiency in GC cells was analyzed by Western blot and quantified as relative protein expression of *CPNE8*/GAPDH. (C) The knockdown and transfection efficiency of *CPNE8* in GC cells was confirmed by qRT-PCR. The expression of mRNAs was calculated using the  $2^{-\Delta\Delta Ct}$  method. (D) CCK-8 assay showed significant differences in GC cell proliferation with knockdown or overexpression of *CPNE8*, respectively. (E) A colony formation assay assessed the effect of *CPNE8* on GC cell proliferation. Colonies were stained with crystal violet, and the number of colonies was counted and shown in a column diagram. Error bars represent mean  $\pm$  SD from three independent experiments. (F) EDU staining of proliferating cells. GC cells were analyzed using a fluorescence microscope (Olympus-Microsystems). DNA (blue) was stained with Hoechst. Cyan cells show EDU/Hoechst-positive cells. The column diagram represented the proliferation rates in various GC cells. Data are presented as mean  $\pm$  SD for at least three independent experiments. (G) Cell cycle analysis in GC cells with respective knockdown or overexpression of *CPNE8*. The bar charts represented the proportion of cells in various cell cycle phases in GC cells. Data are presented as mean  $\pm$  SD for at least three independent experiments. (H) Analysis of apoptosis in GC cells with knockdown or overexpression of *CPNE8*. The proportion of apoptotic cells in GC cells was also shown as column graphs. Data are presented as mean  $\pm$  SD for at least three independent experiments.

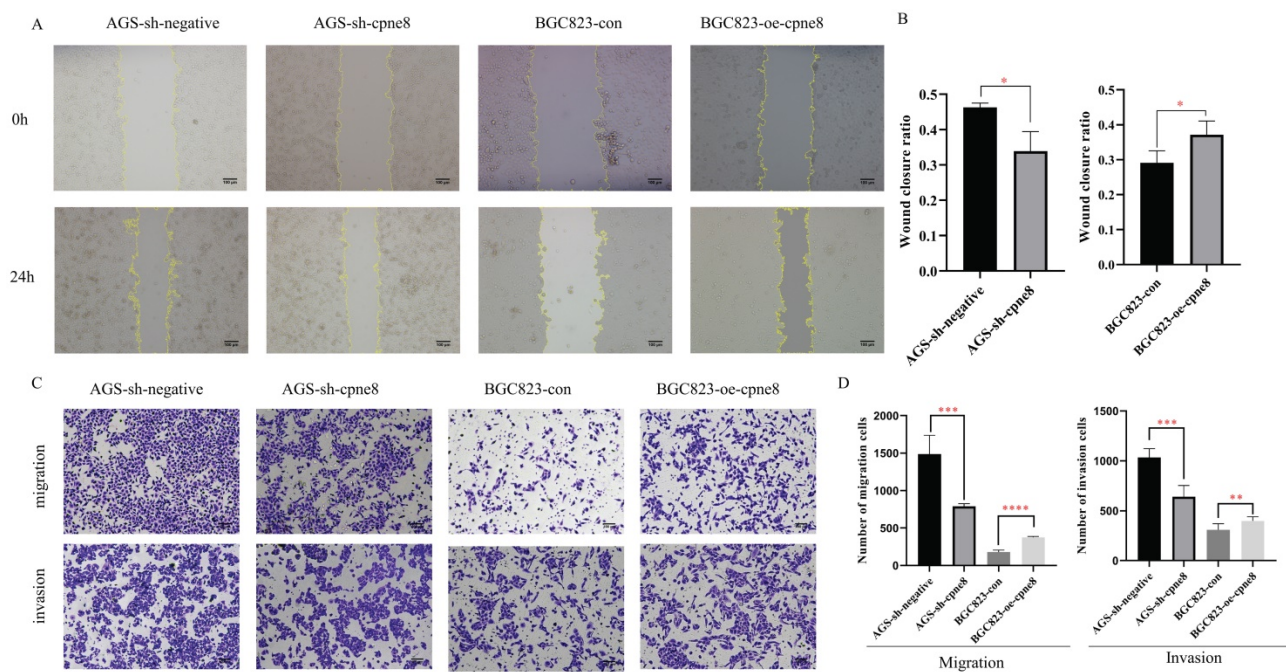


**Figure 3.** *CPNE8* promoted GC cell migration and invasion *in vitro*. **(A)** Wound-healing assays revealed that stably suppressed *CPNE8* expression inhibited migration of GC cells *in vitro*, whereas elevated *CPNE8* expression had the opposite effects. **(B)** Quantitative analysis of wound closure. **(C)** Transwell assays showed that knockdown of *CPNE8* reduced the migration and invasion of GC cells while overexpression of *CPNE8* enhanced the migration and invasion ability of the GC cells. **(D)** Quantitative analysis of migration and invasion of GC cells. Data are presented as mean values  $\pm$  SD of three independent experiments.

Focal adhesion has been recognized as an essential step in cancer cell migration and invasion, and can activate several signaling pathways through phosphorylation and protein-protein interactions that promote tumorigenesis and metastasis [35, 38]. To explore whether *CPNE8*-mediated metastasis of GC was regulated through focal adhesion, we examined the expression of *FAK* and the target gene *ERK* at the mRNA and protein levels by qRT-PCR and western blotting, respectively. Our results revealed that knockdown of *CPNE8* in AGS cells markedly decreased *FAK*, p-*FAK*, total *Erk1/2*, and p-*ERK* expression at both the mRNA and protein levels. By contrast, BGC823 cells overexpressing *CPNE8* exhibited significantly increased *FAK* and p-*FAK* at both the mRNA and protein levels, and increased p-*ERK* mRNA and protein levels, but with no significant change in total *Erk1/2* (Figure 4B-C). To determine the effect of the focal adhesion pathway on gastric carcinogenesis and metastasis, we used siRNA and the *FAK* inhibitor GSK2256098 to treat *CPNE8* overexpressed BGC823 cell lines to detect cell proliferation, motility, and invasiveness, respectively. We treated BGC823-oe-*CPNE8* cells with different concentrations (0–10  $\mu$ M) of GSK2256098 and incubated them at 37 °C for 2 h before detecting the expression levels of *FAK* by Western blotting. We found that treatment with GSK2256098 at a concentration of 10  $\mu$ M significantly reduced *FAK* levels (Supplementary Figure S3C). Therefore, this concentration was selected for subsequent inhibitor

assays. We also examined *FAK* levels by Western blotting to verify the knockdown efficiency of si-*FAK* (Supplementary Figure S3D).

We performed an EDU staining experiment to demonstrate the effect of attenuated *FAK* expression on proliferative capability. As shown in Figure 4D, the result illustrated that the growth capacity of BGC823-oe-*CPNE8* cells decreased after knockdown of *FAK* or GSK2256098 treatment. In addition, we conducted cell cycle and apoptosis experiments to demonstrate the influence of tumor carcinogenesis with after weakening *FAK* expression. As shown in Supplementary Figure S4A, elevated *CPNE8* had no effect on the cell cycle with GSK2256098 treatment or knockdown of *FAK*. After knockdown of *FAK* expression, there was a slight increase apoptotic cells in BGC823-oe-*CPNE8* cells, while no apoptosis was induced by inhibitor treatment (Supplementary Figure S4B). These results suggested that *CPNE8* might participate in other pathways to regulate cell growth.

The wound-healing assay showed that the mobility of BGC823-oe-*CPNE8* cells was diminished in cells treated with si-*FAK* and GSK2256098 (Figure 4E). Furthermore, the Transwell assay showed that GSK2256098 reversed the *CPNE8*-induced migration and invasion abilities of GC cells (Figure 4F), and similar findings were observed after knockdown of *FAK* with si-*FAK*. These results indicate that the focal adhesion pathway mediates *CPNE8*-induced cell migration and invasion, which can be entirely

reversed by the *FAK* inhibitor GSK2256098 or knockdown of *FAK*. In addition, we tested the effect of *CPNE8* on cell adhesion by using an adhesion assay. As shown in **Figure 4G**, knockdown of *CPNE8* in AGS cells resulted in significantly fewer adherent cells than in control cells. In contrast, the overexpression of *CPNE8* in BGC823 cells enhanced their ability to

adhere to the stroma. Consistently, treatment with GSK2256098 or siRNA targeting *FAK* resulted in significant reductions in the number of adherent BGC823-oe-*CPNE8* cells. These results strongly supported our conclusion that *CPNE8* promotes GC metastasis via upregulation of the focal adhesion pathway.

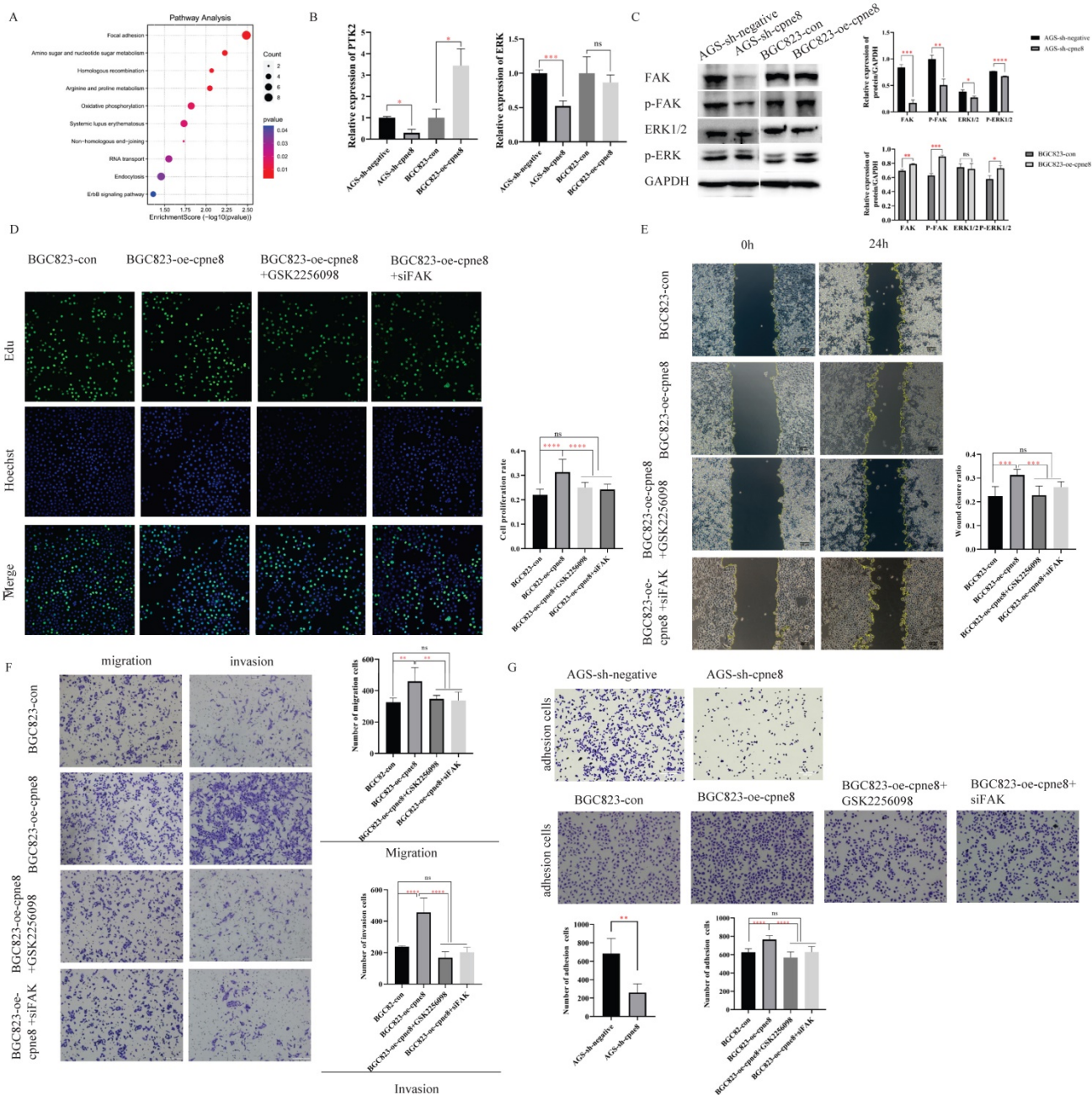


**Figure 4.** *CPNE8* acted on the Focal adhesion pathway to promote GC metastasis. **(A)** KEGG functional enrichment analysis revealed a significant correlation between *CPNE8* expression and Focal adhesion pathway in AGS-sh-*CPNE8* cells compared to the control cells. **(B)** There are relative changes of *FAK* (Gene Symbol as PTK2) and ERK mRNA levels in GC cells with knockdown or overexpression of *CPNE8*. **(C)** Western blot analysis of *FAK*, p-*FAK*, total Erk1/2, and p-ERK protein expression in GC cells with knockdown or overexpression of *CPNE8*. Relative protein expression (interested protein/*GAPDH*) was also quantified in GC cells. **(D)** EDU staining assay showed the proliferating cells with or without diminishing *FAK* expression, such as GSK2256098 treatment and knockdown of *FAK*. Photos were captured using a fluorescence microscope (Leica-Microsystems). DNA (blue) was stained with Hoechst. Cyan cells showed EDU/Hoechst-positive cells. The column diagram represented the proliferation rates in various GC cells. Data are presented as mean  $\pm$  SD for at least three independent experiments. **(E)** Wound-healing assays revealed that both GSK2256098 and si-*FAK* could quantitatively reduce the *CPNE8*-induced migration in BGC823 cells using Image J software. **(F)** Transwell assays confirmed that GSK2256098 or knocking down *FAK* could inhibit migration and invasiveness of GC cells with overexpression of *CPNE8*. **(G)** The representative images showed the adhesion ability of GC cells with knockdown or overexpression of *CPNE8* compared to the control cells and the attenuation of BGC823-oe-*CPNE8* with GSK2256098 or knockdown of *FAK*. The number of GC cells shown in the bar graph that adhered to the plates coated after 2h of incubation was quantified using Image J software.

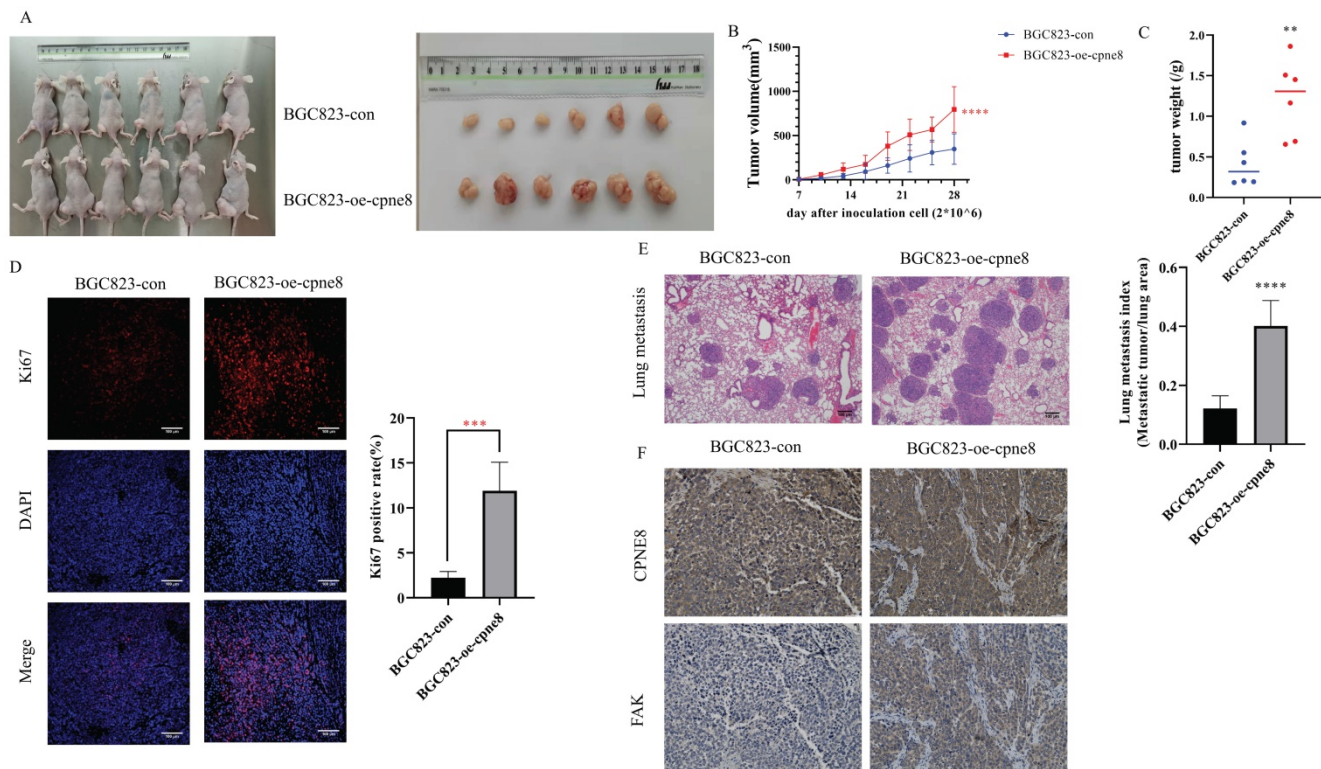


**Figure 5.** *CPNE8* overexpression enhanced GC metastasis *in vivo*. (A) The representative image demonstrated the tumor-bearing mice subcutaneously injected with BGC823 cells overexpressing *CPNE8* versus control mice and the tumors harvested from the nude mice. (B) Tumor volumes were recorded every 3 days. Data are represented as mean  $\pm$  SD of five mice in each group. (C) Significant increase in tumor weight of mice with overexpression of *CPNE8*. (D) Immunofluorescence staining of the proliferation marker revealed a higher expression of Ki67 in tumors overexpressing *CPNE8*. (E) Representative images of HE staining of lungs were collected from mice injected with GC cells via tail vein. Results are also expressed as metastatic lung index (lung tumor area/total lung area) analyzed in mice bearing the metastasis. (F) Immunohistochemistry staining of *CPNE8* and *FAK* in GC tissues harvested from the xenograft mice.

### CPNE8 overexpression enhances GC metastasis *in vivo*

The effect of *CPNE8* on GC metastasis was investigated *in vivo*. Mice injected with BGC-823-oe-*CPNE8* cells showed a significant increase in tumor size and growth at 4 weeks post-inoculation compared to those injected with control cells (Figure 5A-B). After sacrificing the mice, tumor tissues were weighed. The group with *CPNE8* overexpression showed a significant increase in tumor weight (Figure 5C). Immunofluorescence staining confirmed that tumors derived from the BGC823-oe-*CPNE8* group exhibited higher Ki67 expression levels than tumors derived from control cells (Figure 5D). This implies that *CPNE8* could improve the proliferative capacity of tumors *in vivo*. To further define the role of *CPNE8* expression in promoting metastasis *in vivo*, we injected BGC823 cells with *CPNE8* overexpression into nude mice through the tail vein. All mice were sacrificed four weeks later to harvest the lungs for H&E staining. Nude mice inoculated with *CPNE8* overexpressing BGC823 cells exhibited more metastatic lung nodules (Figure 5E). Immunohistochemical analysis showed a consistent trend of *CPNE8* and *FAK* expression in GC tissues of xenograft mice.

IHC staining confirmed that tumors derived from the BGC823-oe-*CPNE8* group exhibited higher *CPNE8* and *FAK* expression levels than tumors derived from control cells (Figure 5F). Taken together, these *in vivo* experiments verified that *CPNE8* was essential for promoting the growth and metastasis of GC cells.

### Influence of high *CPNE8* expression on the infiltration of CAFs in GC

Interactions between tumor cells and tumor microenvironment (TME) dynamically regulate the metastatic process [39-41]. We reanalyzed the TCGA-STAD dataset using the ESTIMATE algorithm and calculated the stromal score, immune score, and tumor purity (Figure 6A). The results showed that the stromal score ( $p < 0.001$ ), immune score ( $p < 0.01$ ), and ESTIMATE score ( $p < 0.001$ ) were significantly higher in the high *CPNE8* expression cluster (Figure 6A). Consistently, we found that high *CPNE8* expression was associated with higher stromal, immune, and ESTIMATE scores compared to the low *CPNE8* group in GSE84437 (Supplementary Figure S5A).

Cancer-associated fibroblasts (CAFs), the most prominent and abundant cell type in the GC stroma, are activated fibroblasts that play a key role in GC progression and metastasis [42-44]. We used multiple

algorithms to compare the association between CAFs infiltration and *CPNE8* expression. Consistent results demonstrated a high correlation between *CPNE8* and CAF infiltration in the TCGA-STAD cohort (**Figure 6B**) and GSE84437 (Supplementary Figure S5B). These results suggest that *CPNE8* may manipulate the recruitment of CAFs into the tumor microenvironment. IHC staining verified that tissues in xenograft mice overexpressing *CPNE8* exhibited high expression of  $\alpha$ -SMA, a well-known CAF marker (**Figure 6C**). In addition, we performed the correlation analysis between *CPNE8* expression and several activated CAFs biomarkers in the TCGA-STAD cohort, such as  $\alpha$ -smooth muscle actin ( $\alpha$ -SMA, *ACTA2*), fibroblast-specific protein-1 (FSP-1, *S100A4*), fibroblasts activated protein (*FAP*), Thy-1 (*THY1*), (*PDPN*), and integrin beta1 (*ITGB1*). As shown in **Figure 6D**, there were significant positive correlations between *CPNE8* and activated CAFs biomarkers, such as *ACTA2* ( $R = 0.42, p = 3.7e-19$ ), *FAP* ( $R = 0.35, p = 3.4e-13$ ), *ITGB1* ( $R = 0.48, p = 1.1e-24$ ), *PDPN* ( $R = 0.38, p = 3.4e-15$ ), *S100A4* ( $R = 0.15, p = 0.0017$ ), and *THY1* ( $R = 0.37, p = 7e-15$ ). CAFs always secrete cytokines, chemokines, and growth factors in the tumor microenvironment to promote tumor progression and migration [45-47]. To test this in our model, we analyzed the correlation between *CPNE8* and various chemokines and chemokine receptors using the TISIDB database. As shown in **Figure 6E**, there were significant positive correlations between *CPNE8* and chemokines secreted from CAFs, such as *CCL2* ( $R = 0.282, p = 6.24e-09$ ), *CCL11* ( $R = 0.203, p = 3.33e-05$ ), and *CXCL12* ( $R = 0.292, p = 1.67e-09$ ). We also observed a correlation between *CPNE8* expression and chemokine receptors, including *CXCR4* ( $R = 0.285, p = 3.98e-09$ ) and *CCR4* ( $R = 0.207, p = 2.27e-05$ ). We used qRT-PCR analysis to verify the correlation between *CPNE8* and chemokine receptor binding to the chemokines secreted by CAFs. The results showed that knockdown of *CPNE8* resulted in a significant decrease in the expression of *CXCR4* and *CCR4* in GC cells compared to control cells, while overexpression of *CPNE8* resulted in an upregulation of these genes (**Figure 6F**). These findings suggested that high *CPNE8* expression may affect the infiltration of cancer-associated fibroblasts.

### Higher expression of *CPNE8* was correlated with poorer immunotherapy efficacy

Immune cells in the tumor microenvironment (TME) play an essential role in tumor progression [48]. We used the MCP-counter algorithm to analyze the relationship between *CPNE8* expression and immune cell infiltration and found high correlations between *CPNE8* expression and monocyte, macro-

phage/monocyte, myeloid dendritic cell, and neutrophil cell infiltration (**Figure 7A**). In addition, we used the "ssGSEA" algorithm to calculate the absolute enrichment of immune pathways in each sample and found that signaling pathways involved in immune responses, such as B cells, DCs, macrophages, MHC class I, Type I IFN Reponse, and Type II IFN Reponse, were enriched in the high *CPNE8* expression cluster (**Figure 7B**). To further elucidate the role of *CPNE8* in immunotherapy, as represented by immune checkpoint blockades (CB), we extended our analysis to the association of *CPNE8* with several well-known biomarkers. Spearman's correlation analysis of the TCGA-STAD cohort revealed that *CPNE8* expression was significantly negatively correlated with MSI ( $R = -0.25, p = 8.87e-07$ ) and TMB ( $R = -0.36, p = 9.62e-13$ ), implying a poor response to immunotherapy (Supplementary Figure S6A-B). In the TCGA-STAD cohort, *CPNE8* expression was positively correlated with the expression of immune checkpoint genes such as *PDCD1LG2*, *HAVCR2*, and *TIGIT*, suggesting that higher *CPNE8* expression may predict poorer immune responses in GC patients (**Figure 7C**). Furthermore, using the TIDE database (<http://tide.dfci.harvard.edu>), we calculated the correlations of *CPNE8* with dysfunction and TIDE scores and found that increased *CPNE8* expression was associated with higher immune dysfunction ( $R = 0.19, p = 0.00025$ ) (**Figure 7D**) and TIDE scores ( $R = 0.19, p = 0.00025$ ) (**Figure 7E**). Consistently, high *CPNE8* expression predicted adverse responses to immune checkpoint therapy in GC patients (efficiency 30.32% vs. 44.39%,  $p = 0.0049$ ) (**Figure 7F**). These results suggest that *CPNE8* expression can predict the clinical benefits of ICB in STAD.

## Discussion

Tumor metastasis, the leading cause of death in patients with advanced GC, remains a poorly understood cause of tumor progression [6, 9]. Therapeutic efficacy for metastatic GC remains limited owing to the poor prognosis of patients [49]. Accumulating evidence suggests that CPNE family members are involved in tumorigenesis and metastasis. However, the role of *CPNE8* in GC progression and metastasis has not yet been thoroughly evaluated. Furthermore, tumor metastasis is not only driven by the accumulation of intrinsic changes within malignant cells, but is also modulated by various immune and stromal components in the tumor microenvironment [50-52]. Therefore, the aim of this study was to explore the potential mechanisms of *CPNE8* in the progression and metastasis of GC and its potential immune activation and sensitivity to immunotherapies of GC patients.

Our research revealed that *CPNE8* is highly expressed in GC, with significantly higher expression in metastatic tumors, especially in patients with liver metastases. In addition, *CPNE8* was highly expressed in patients with advanced tumors (with a progressive grade or advanced TNM stage), suggesting that patients with high *CPNE8* expression exhibit more aggressive clinicopathological characteristics. *CPNE8* could be used as an independent prognostic factor for GC, and higher *CPNE8* expression predicted poorer prognosis in GC. Summarily, *CPNE8* may serve as a novel prognostic marker for GC. We knocked down or overexpressed *CPNE8* in GC cells. *In vitro* and *in vivo*

*in vivo* functional assays revealed that knockdown of *CPNE8* reduced cell proliferation, possibly by promoting apoptosis and inhibiting the G1/S phase of cells. In contrast, overexpression of *CPNE8* promoted cell proliferation by facilitating transition from the G1/S phase. Moreover, our results showed that GC cells with high *CPNE8* expression demonstrated enhanced invasion and migration abilities, thus providing a basis for tumor metastasis. *In vivo*, *CPNE8* promoted the growth and metastasis of xenograft tumors, which was consistent with the results obtained *in vitro*.

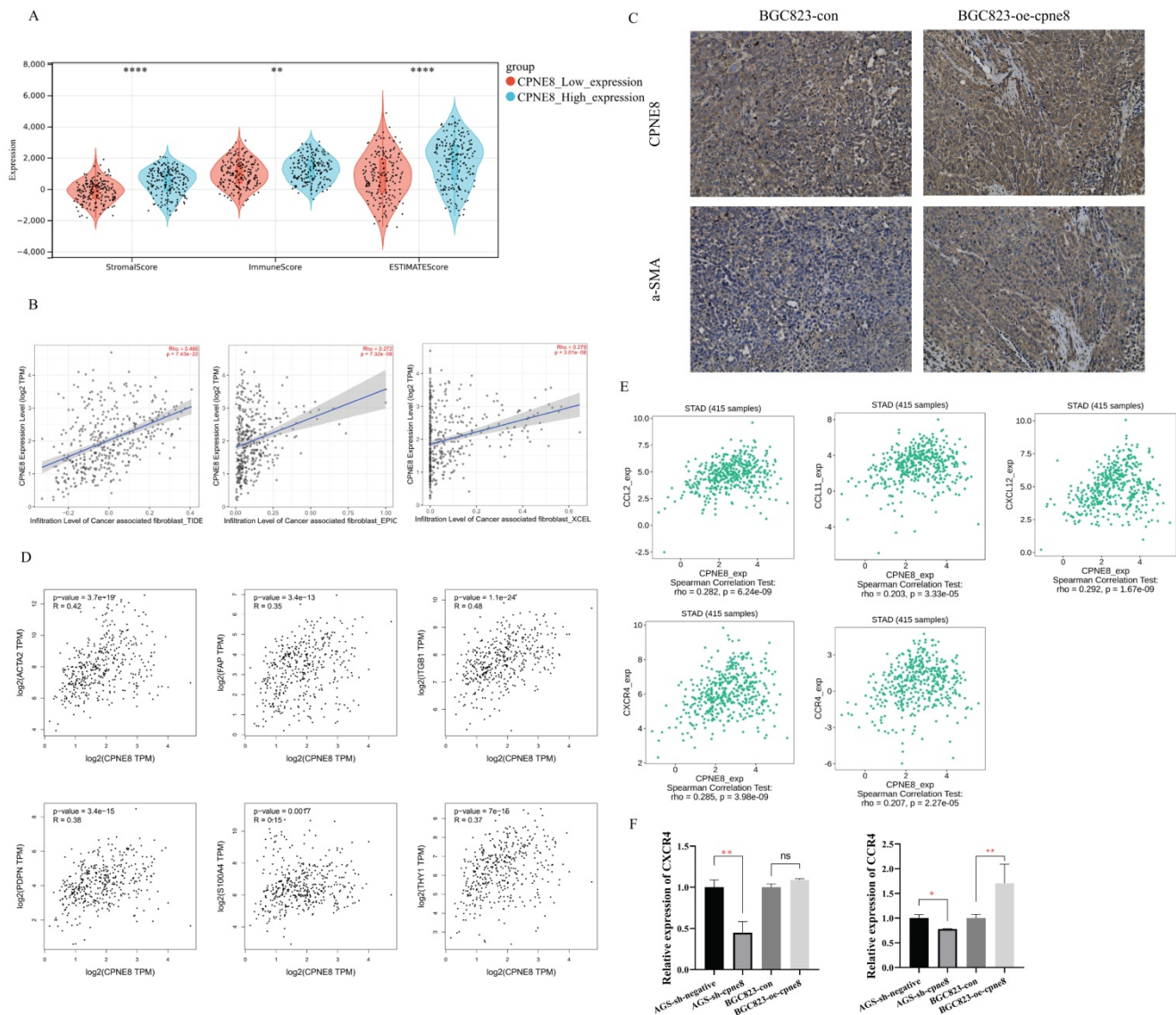


**Figure 6.** High expression of *CPNE8* was associated with the infiltration of cancer-associated fibroblasts in GC. **(A)** Manipulated Stroma score, Immune score, and ESTIMATE score based on *CPNE8* status in TCGA-STAD cohort. **(B)** The correlation of *CPNE8* expression and the infiltration of CAFs was quantified using the TIDE, EPIC, and XCELL algorithm in the TCGA-STAD cohort in the TIMER2 database. Each dot represents one sample. **(C)** Immunohistochemistry staining of *CPNE8* and a-SMA in GC tissues of xenograft mice. **(D)** Significant and positive correlations between *CPNE8* expression and *ACTA2*, *FAP*, *ITGB1*, *PDPN*, *S100A4*, and *THY1*. **(E)** The correlation of *CPNE8* expression with various chemokines or chemokine receptors was displayed using the TISIDB database. **(F)** The mRNA levels of chemokine receptors were quantified by qRT-PCR in GC cells with respective knockdown or overexpression of *CPNE8* compared to the control cells.

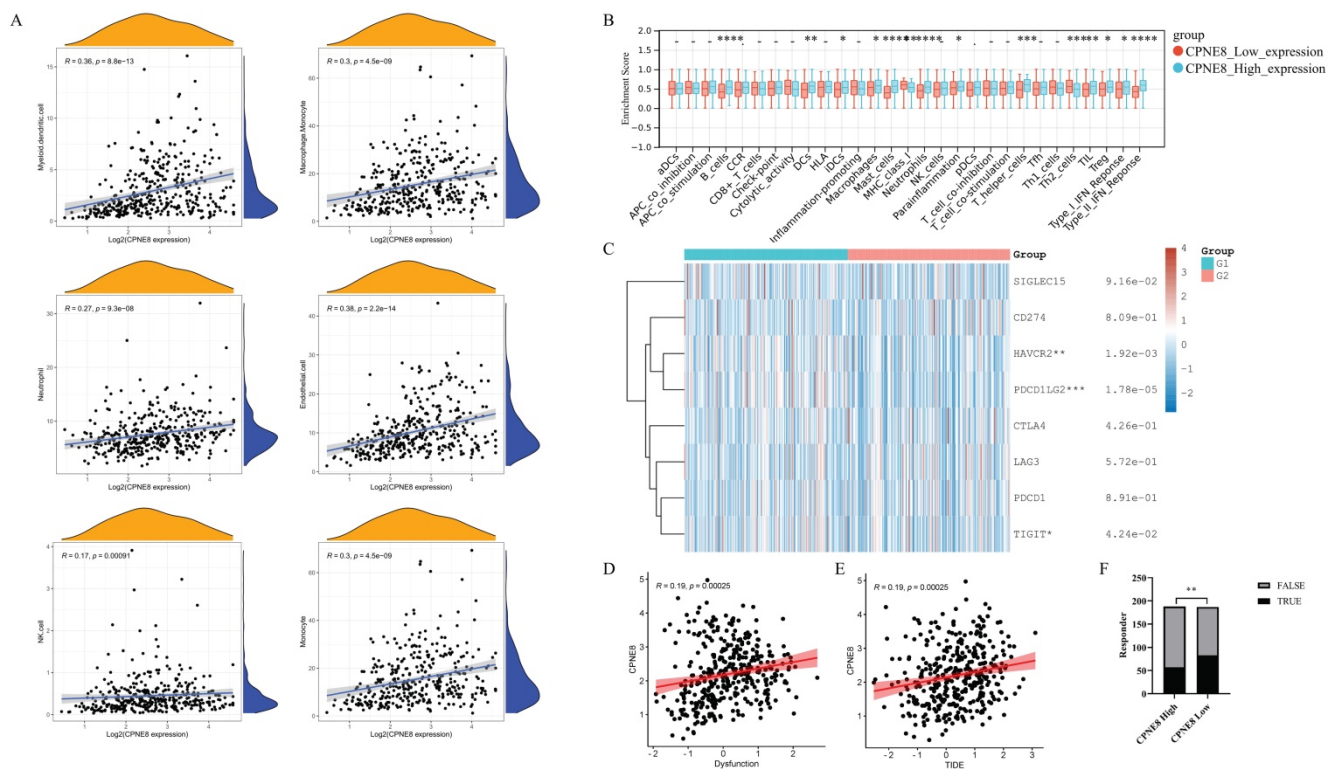


**Figure 7.** *CPNE8* expression could predict the clinical benefit of ICB. (A) Correlation of *CPNE8* expression and immune infiltrating cells quantified using the MCP-counter algorithm in the TCGA-STAD cohort. (B) Correlation between ssGSEA scores of 29 immune cells and *CPNE8* expression in gastric cancer. (C) The heatmap showed the correlation between *CPNE8* expression and immune checkpoint genes. G1 represented the *CPNE8* high expression group; G2 represented the *CPNE8* low expression group. (D) Increased *CPNE8* expression was associated with higher immune dysfunction scores. (E) The mRNA expression of *CPNE8* was positively correlated with the TIDE score. (F) The rate of immune checkpoint blockade responses in GC patients was predicted by the TIDE algorithm in the high or low *CPNE8* groups.

We further analyzed the mechanism of *CPNE8* in enhancing GC metastasis. First, the GSEA and KEGG results showed that the high *CPNE8* expression group was functionally enriched in focal adhesion, gap junction, and ECM receptor interaction in the TCGA-STAD cohort, which were correlated with cancer metastasis [35-37]. Our mass spectrometry analysis confirmed that *CPNE8* is closely associated with focal adhesions. The role of focal adhesion in cell adhesion, migration, and cancer invasiveness has been well-studied [35, 53, 54]. The tyr397 phosphorylation and kinase activity of *FAK* were critical for GC invasiveness [55]. *ERK* is a member of the mitogen-activated protein kinase (*MAPK*) family and is activated by *FAK* interactions [56, 57]. Our study demonstrated that *CPNE8* enhanced GC cell migration and invasion in an *FAK*-dependent manner. The phosphorylation levels of *FAK* (Tyr397) and *ERK* (p42/p44) decreased in cells with *CPNE8* knockdown and increased in cells with *CPNE8* overexpression. GSK2256098, a small molecule *FAK* inhibitor, reversed *CPNE8*-induced GC cell proliferative capability, mobility, and invasiveness. The proliferative capability of GC cells decreased after GSK2256098 treatment or knocking down *FAK*. However, there were no significant differences in the cell cycle and apoptosis between BGC823-oe-*CPNE8* cells with and

without the *FAK* inhibitor. Based on the findings from cell cycle and apoptosis analyses, knockdown of *CPNE8* led to G1-S phase delay and apoptosis, while overexpression of *CPNE8* promoted the cell cycle, suggesting that *CPNE8* may regulate the G1-S phase transition and cell apoptosis via alternative pathways to focal adhesion.

We further studied tumor cell adhesion using fibronectin, an essential component for the adhesion of many cell types [58]. While our results showed that *CPNE8* promoted GC cell adhesion, which could be reduced by *FAK* inhibitor, the underlying molecular mechanism between *CPNE8* and *FAK* is still unknown. Nevertheless, our results suggest that *CPNE8* plays a carcinogenic role in GC by activating the focal adhesion pathway, and *FAK* inhibition may be a promising therapy for GC patients with high *CPNE8* expression.

Several studies have reported that the tumor immune microenvironment, consisting of immune cells, inflammatory cells, and CAFs, is associated with the invasion and metastasis of multiple tumor cells, and is closely correlated with tumor prognosis [50, 51]. CAFs, critical components of the stroma, have been reported to regulate chemokines in the tumor microenvironment and promote the progression of tumor metastasis [45, 46]. Our results demonstrated

that *CPNE8* was positively correlated with CAFs using different algorithms in TCGA-STAD and GSE84437 cohorts. IHC analysis results also revealed that overexpression of *CPNE8* in GC tissue exhibited higher  $\alpha$ -SMA expression, an evidential marker of CAFs, which implied that *CPNE8* overexpression might recruit more CAFs in the microenvironment to promote GC metastasis. It has been previously demonstrated that CAFs secrete *CXCL12*, thus stimulating *CXCL12/CXCR4* signaling and promoting tumor growth and angiogenesis in GC [59]. Previous studies also showed that CAFs could produce the chemokine ligand *CCL17* to act on *CCR4* of cancer cells to improve cancer proliferation and migration [60]. In addition, Tsuyada et al. showed that *CCL2* and *CXCL14* secreted by CAFs can increase the recruitment of macrophages and promote the invasive ability of breast cancer [61]. Nieh et al. found that CAFs facilitate cancer invasiveness through paracrine effects on micro-environmental *CCL11* signaling in oral squamous cell carcinoma [62]. Our study revealed significant correlations between *CPNE8* expression and chemokines secreted from CAFs in the TCGA-STAD cohort using the TISIDB database.

Interestingly, we assessed the mRNA levels of the chemokine receptors *CCR4* and *CXCR4* in GC cells and found that knockdown or overexpression of *CPNE8* significantly regulated their expression, implying that *CPNE8* may affect the function of CAFs via modulation of chemokine binding to cancer cells. However, whether mutual regulation between *CPNE8* and CAFs exists is still unclear. The potential regulatory mechanism between *CPNE8* and CAFs warrants more in-depth study, which may contribute to the understanding of additional mechanisms involved in GC metastasis.

Multiple tumor immune infiltrating cells, such as macrophages, MDSC, granulocytes, and lymphocytes, have been reported to promote multiple tumor metastases [39, 63]. In this study, we showed that *CPNE8* expression is significantly positively correlated with monocytes, macrophages/monocytes, myeloid dendritic cells, and neutrophils. Functional enrichment by “ssGSEA” also demonstrated the involvement of *CPNE8* in immune-related pathways.

Tumor immunotherapy is a powerful and promising clinical approach for the treatment of patients with cancer. However, the response rate remains challenging to assess in tumors, including in patients with GC [64, 65]. An increasing number of biomarkers are used to predict immune response, and these biomarkers play vital roles in the development, metastasis, and treatment of cancer [66, 67]. Microsatellite instability (MSI) is the first pan-cancer biomarker approved for immune checkpoint blockade

(ICB) therapy [68, 69]. MSI-induced shift mutations result in the generation of large neoantigens, and tumors with high mutation rates may respond well to checkpoint inhibitors (CPIs) [70]. TMB has been reported as an effective biomarker of immune checkpoint inhibitor sensitivity [71]. Tumors with high TMB typically have higher levels of immune system-recognizable neoantigens that correlate with the response to PD-1, PD-L1, and CTLA-4 blockade immunotherapy [71, 72]. In this study, we observed a significant negative correlation between *CPNE8* expression and MSI/TMB, implying a poor immune response in GC patients with high *CPNE8* expression. Although the immune system can recognize malignant cells, the inactivation of anti-tumor T cells due to the upregulation of suppressive immune checkpoints in the tumor microenvironment results in an ineffective immune system response to the tumor cells [73]. We found that *CPNE8* expression was positively correlated with the expression of suppressive checkpoints—*HAVCR2*, *PDCD1LG2*, and *TIGIT*. Peng et al. designed a new computational framework, the TIDE score, to assess the status of tumor immunity and predict the effect of immunosuppressive therapy [28, 29]. *CPNE8* expression was positively correlated with immune dysfunction and TIDE scores in our study. By contrast, the response rate to immune checkpoint therapy was reduced by 14.07% in the *CPNE8* high-expression group. These results suggest that GC patients with high *CPNE8* expression may benefit less from available immune blockade therapy.

Our findings establish a novel link between *CPNE8* expression and GC progression. *CPNE8* might promote tumor proliferative capacity by accelerating the G1-S phase transition of the cell cycle. Conversely, knockdown of *CPNE8* could lead to G1-S phase blockade to induce apoptosis, an outcome of cell cycle arrest [74-76]. In addition, *CPNE8*, a critical core factor of tumor metastasis, triggers the focal adhesion pathway by upregulating *FAK* and *ERK* expression and activating CAFs in the tumor microenvironment by regulating chemokines and their receptors, leading to a suppressed immune response.

Our study had some limitations, we did not elucidate the molecular mechanism of *FAK* regulation by *CPNE8* and how *CPNE8* activates CAFs. While studies concerning *FAK* activation in CAFs have been reported [77, 78], it is worthwhile to further investigate whether *CPNE8* is involved in this regulatory effect.

In conclusion, our findings suggest that *CPNE8* represents an independent prognostic risk factor that can predict poor outcomes in GC. *CPNE8* could affect the migration and invasion of GC cells by enhancing

focal adhesion, thus identifying a promising therapeutic target for GC. Furthermore, high levels of *CPNE8* can recruit more CAFs and involve immune pathways in the tumor microenvironment. Together, these findings may help develop more effective therapeutic strategies by targeting GC progression and metastasis.

## Abbreviations

AUC: area under curve; CAFs: cancer associated fibroblasts; CAMs: cell adhesion molecules; CPI: checkpoint inhibitor; CPN: copine; DFS: disease-free survival; FAK: focal adhesion kinase; FAP: fibroblast-activated protein; FBS: fetal bovine serum; FSP: fibroblast-specific protein; GC: gastric cancer; GES1-: gastric mucosal epithelial cell line; GO: gene ontology; GSEA: gene-set enrichment analysis; ICB: immune checkpoint blockade; ITGB1: integrin beta 1; KEGG: Kyoto encyclopedia of genes and genomes; MAPK: mitogen-activated protein kinase; MSI: microsatellite instability; OS: overall survival; PDPN: podoplanin; PFS: progression-free survival; ROC: receiver operating characteristic; ssGSEA: single-sample gene set enrichment analysis; STAD: clinical data of stomach adenocarcinoma; TIDE: tumor immune dysfunction and exclusion; TME: tumor microenvironment.

## Supplementary Material

Supplementary figures and tables.  
<https://www.ijbs.com/v18p4932s1.pdf>

## Acknowledgements

We sincerely acknowledge the contributions from the TCGA project and the GEO datasets.

## Funding

This research was funded by the Natural Science Foundation of Guangdong Province, China (No. 2021A1515011113, Lin Lu), Guangzhou Science and Technology Program (No. 201904010427, Lin Lu), and Guangzhou General Science and technology project of Health and Family Planning (grant number 20201A011007, Lin Lu), and partially supported by the Longenbaugh Foundation (Qiao Li).

## Availability of data and material

Publicly available datasets were analyzed in this study. This data can be found at the GEO browser ("<https://www.ncbi.nlm.nih.gov/geo/>") and TCGA project ("<https://portal.gdc.cancer.gov/>").

## Author contributions

Guolong Liu and Lin Lu designed the study. Peiling Zhang and Xiaofei Cao performed the

experimental manipulations, analyzed the data, and wrote the manuscript. Mingmei Guan and Dailing Li performed the experiments. Hong Xiang integrated the data. Qian Peng and Yun Zhou performed animal experiments. Chengyin Weng processed the data into graphs. Xisheng Fang analyzed data by software. Xia Liu did the investigation. Haibo Mao did the investigation. Mingmei Guan and Xiaofei Cao did the investigation. Lin Lu, Guolong Liu, and Qiao Li wrote the manuscript. Lin Lu was responsible for the manuscript review. All authors read and approved the final manuscript.

## Competing Interests

The authors have declared that no competing interest exists.

## References

- Sung H, Ferlay J, Siegel RL, Laversanne M, Soerjomataram I, Jemal A, et al. Global Cancer Statistics 2020: GLOBOCAN Estimates of Incidence and Mortality Worldwide for 36 Cancers in 185 Countries. *CA Cancer J Clin.* 2021; 71: 209-49.
- Chen W, Zheng R, Baade PD, Zhang S, Zeng H, Bray F, et al. Cancer statistics in China, 2015. *CA Cancer J Clin.* 2016; 66: 115-32.
- Ferlay J, Colombet M, Soerjomataram I, Parkin DM, Pineros M, Znaor A, et al. Cancer statistics for the year 2020: An overview. *Int J Cancer.* 2021; 149: 778-89.
- Lu L, Mullins CS, Schafmayer C, Zeißig S, Linnebacher MJCC. A global assessment of recent trends in gastrointestinal cancer and lifestyle-associated risk factors. *Cancer Communications.* 2021; 41: 1137-51.
- Wang FH, Zhang XT, Li YF, Tang L, Qu XJ, Ying JE, et al. The Chinese Society of Clinical Oncology (CSCO): Clinical guidelines for the diagnosis and treatment of gastric cancer, 2021. *Cancer Commun (Lond).* 2021; 41: 747-95.
- Bilici A. Treatment options in patients with metastatic gastric cancer: current status and future perspectives. *World J Gastroenterol.* 2014; 20: 3905-15.
- Digkila A, Wagner AD. Advanced gastric cancer: Current treatment landscape and future perspectives. *World J Gastroenterol.* 2016; 22: 2403-14.
- Sexton RE, Al Hallak MN, Diab M, Azmi AS. Gastric cancer: a comprehensive review of current and future treatment strategies. *Cancer metastasis reviews.* 2020; 39: 1179-203.
- Riihimäki M, Hemminki A, Sundquist K, Sundquist J, Hemminki KJO. Metastatic spread in patients with gastric cancer. *Oncotarget.* 2016; 7: 52307.
- Creutz CE, Tomsig JL, Snyder SL, Gautier M-C, Skouri F, Beisson J, et al. The copines, a novel class of C2 domain-containing, calcium-dependent, phospholipid-binding proteins conserved from Paramecium to humans. *Journal of Biological Chemistry.* 1998; 273: 1393-402.
- Tomsig JL, Creutz CE. Biochemical characterization of copine: a ubiquitous Ca<sup>2+</sup>-dependent, phospholipid-binding protein. *Biochemistry.* 2000; 39: 16163-75.
- Tang H, Pang P, Qin Z, Zhao Z, Wu Q, Song S, et al. The CPNE family and their role in cancers. *Frontiers in Genetics.* 2021; 12.
- Arteta MY, Kjellman T, Bartesaghi S, Wallin S, Wu X, Kvist AJ, et al. Successful reprogramming of cellular protein production through mRNA delivered by functionalized lipid nanoparticles. *Proceedings of the National Academy of Sciences.* 2018; 115: E3351-E60.
- Ilaqua AN, Price JE, Graham BN, Buccilli MJ, McKellar DR, Damer CK. Cyclic AMP signaling in Dictyostelium promotes the translocation of the copine family of calcium-binding proteins to the plasma membrane. *BMC Cell Biol.* 2018; 19: 13.
- Mukhopadhyay S, Badgandi HB, Hwang SH, Somatilaka B, Shimada IS, Pal K. Trafficking to the primary cilium membrane. *Mol Biol Cell.* 2017; 28: 233-9.
- Maitra R, Grigoryev DN, Bera TK, Pastan IH, Lee B. Cloning, molecular characterization, and expression analysis of Copine 8. *Biochemical and biophysical research communications.* 2003; 303: 842-7.

17. Liu S, Tang H, Zhu J, Ding H, Zeng Y, Du W, et al. High expression of Copine 1 promotes cell growth and metastasis in human lung adenocarcinoma. *Int J Oncol.* 2018; 53: 2369-78.
18. Lin H-c, Zhang F-l, Geng Q, Yu T, Cui Y-q, Liu X-h, et al. Quantitative proteomic analysis identifies CPNE3 as a novel metastasis-promoting gene in NSCLC. *Journal of proteome research.* 2013; 12: 3423-33.
19. Ramsey H, Zhang DE, Richkind K, Burcoglu-O'Ral A, Hromas R. Fusion of AML1/Runx1 to copine VIII, a novel member of the copine family, in an aggressive acute myelogenous leukemia with t(12;21) translocation. *Leukemia.* 2003; 17: 1665-6.
20. Zhao Y, Huang J, Liu T, He S, Shang C, Guo L, et al. Overexpression of long non-coding RNA RP11-396F22.1 correlates poor prognosis of patients with early-stage cervical cancer. *Am J Transl Res.* 2018; 10: 684-95.
21. Dang TT, Westcott JM, Maine EA, Kanchwala M, Xing C, Pearson GWJO.  $\Delta$ Np63 $\alpha$  induces the expression of FAT2 and Slug to promote tumor invasion. *Oncotarget.* 2016; 7: 28592.
22. Junfeng Z, Zhiping Z, Huan Q, Bing N, University WHJJoTMM. Copine 8 promotes proliferation, invasion and metastasis of pancreatic cancer. *Journal of Third Military Medical University.* 2020; 42: 601-10.
23. Chiu WC, Lee YC, Su YH, Chai CY, Hu SC, Yuan SF, et al. Correlation of matrix metalloproteinase-2 and -9 expression with recurrences in primary spontaneous pneumothorax patients. *J Thorac Dis.* 2016; 8: 3667-75.
24. Vegesna RJNC. Inferring tumour purity and stromal and immune cell admixture from expression data. *Nat Commun.* 2013; 4: 1-11.
25. Li T, Fu J, Zeng Z, Cohen D, Li J, Chen Q, et al. TIMER2.0 for analysis of tumor-infiltrating immune cells. *Nucleic Acids Res.* 2020; 48: W509-W14.
26. Ru B, Ngar WC, Tong Y, Zhong JY, Zhong S, Wu WC, et al. TISIDB: an integrated repository portal for tumor-immune system interactions. *Bioinformatics.* 2019; 20.
27. Becht E, Giraldo NA, Lacroix L, Biology BBJG. Estimating the population abundance of tissue-infiltrating immune and stromal cell populations using gene expression. *Genome Biology.* 2016; 17.
28. Fu J, Li K, Zhang W, Wan C, Zhang J, Jiang P, et al. Large-scale public data reuse to model immunotherapy response and resistance. *Genome Med.* 2020; 12: 21.
29. Jiang P, Gu S, Pan D, Fu J, Sahu A, Hu X, et al. Signatures of T cell dysfunction and exclusion predict cancer immunotherapy response. *Nat Med.* 2018; 24: 1550-8.
30. Robin X, Turck N, Hainard A, Tiberti N, Lisacek F, Sanchez JC, et al. pROC: an open-source package for R and S+ to analyze and compare ROC curves. *BMC Bioinformatics.* 2011; 12: 77.
31. Li L, Wang T, Li S, Chen Z, Wu J, Cao W, et al. TDO2 Promotes the EMT of Hepatocellular Carcinoma Through Kyn-AhR Pathway. *Frontiers in oncology.* 2021; 10: 3008.
32. Wang X, Li T, Cheng Y, Wang P, Yuan W, Liu Q, et al. CYTL1 inhibits tumor metastasis with decreasing STAT3 phosphorylation. *Oncimmunology.* 2019; 8: e1577126.
33. Huang Z, Zhou JK, Wang K, Chen H, Qin S, Liu J, et al. PDLIM1 inhibits tumor metastasis through activating hippo signaling in hepatocellular carcinoma. *Hepatology.* 2020; 71: 1643-59.
34. Beauchemin N, Arabzadeh A. Carcinoembryonic antigen-related cell adhesion molecules (CEACAMs) in cancer progression and metastasis. *Cancer metastasis reviews.* 2013; 32: 643-71.
35. Zhao J, Guan JL. Signal transduction by focal adhesion kinase in cancer. *Cancer metastasis reviews.* 2009; 28: 35-49.
36. Lu L, Weng C, Mao H, Fang X, Liu X, Wu Y, et al. IL-17A promotes migration and tumor killing capability of B cells in esophageal squamous cell carcinoma. *Oncotarget.* 2016; 7: 21853-64.
37. Eble JA, Niland S. The extracellular matrix in tumor progression and metastasis. *Clin Exp Metastasis.* 2019; 36: 171-98.
38. Cao Q, Mao Z-D, Shi Y-J, Chen Y, Sun Y, Zhang Q, et al. MicroRNA-7 inhibits cell proliferation, migration and invasion in human non-small cell lung cancer cells by targeting FAK through ERK/MAPK signaling pathway. *Oncotarget.* 2016; 7: 77468.
39. Kitamura T, Qian BZ, Pollard JW. Immune cell promotion of metastasis. *Nat Rev Immunol.* 2015; 15: 73-86.
40. Goubran HA, Kotb RR, Stakiw J, Emara ME, Burnouf T. Regulation of tumor growth and metastasis: the role of tumor microenvironment. *Cancer Growth Metastasis.* 2014; 7: 9-18.
41. Ungefroren H, Sebens S, Seidl D, Lehnert H, Hass R. Interaction of tumor cells with the microenvironment. *Cell Commun Signal.* 2011; 9: 18.
42. Zheng H, Liu H, Li H, Dou W, Wang X. Weighted Gene Co-expression Network Analysis Identifies a Cancer-Associated Fibroblast Signature for Predicting Prognosis and Therapeutic Responses in Gastric Cancer. *Front Mol Biosci.* 2021; 8: 744677.
43. Ham IH, Lee D, Hur H. Role of Cancer-Associated Fibroblast in Gastric Cancer Progression and Resistance to Treatments. *J Oncol.* 2019; 2019: 6270784.
44. Yan Y, Wang LF, Wang RF. Role of cancer-associated fibroblasts in invasion and metastasis of gastric cancer. *World J Gastroenterol.* 2015; 21: 9717-26.
45. Hussain S, Peng B, Cherian M, Song JW, Ahirwar DK, Ganju RK. The Roles of Stroma-Derived Chemokine in Different Stages of Cancer Metastases. *Front Immunol.* 2020; 11: 598532.
46. Guo S, Deng CX. Effect of Stromal Cells in Tumor Microenvironment on Metastasis Initiation. *Int J Biol Sci.* 2018; 14: 2083-93.
47. Karagiannis GS, Poutahidis T, Erdman SE, Kirsch R, Riddell RH, Diamandis EPJMcR. Cancer-associated fibroblasts drive the progression of metastasis through both paracrine and mechanical pressure on cancer tissue. *Molecular cancer research.* 2012; 10: 1403-18.
48. Lei X, Lei Y, Li J-K, Du W-X, Li R-G, Yang J, et al. Immune cells within the tumor microenvironment: Biological functions and roles in cancer immunotherapy. *Cancer letters.* 2020; 470: 126-33.
49. Yang D, Hendifar A, Lenz C, Togawa K, Lenz F, Lurje G, et al. Survival of metastatic gastric cancer: Significance of age, sex and race/ethnicity. *J Gastrointest Oncol.* 2011; 2: 77-84.
50. Lunt SJ, Chaudary N, Hill RP. The tumor microenvironment and metastatic disease. *Clin Exp Metastasis.* 2009; 26: 19-34.
51. Anderson NM, Simon MC. The tumor microenvironment. *Curr Biol.* 2020; 30: R921-R5.
52. Justus CR, Sanderlin EJ, Yang LVJlJoms. Molecular connections between cancer cell metabolism and the tumor microenvironment. *International journal of molecular sciences.* 2015; 16: 11055-86.
53. Weiner TM, Liu ET, Craven RJ, Cance WG. Expression of focal adhesion kinase gene and invasive cancer. *Lancet (London, England).* 1993; 342: 1024-5.
54. Wu S, Chen M, Huang J, Zhang F, Lv Z, Jia Y, et al. ORAI2 Promotes Gastric Cancer Tumorigenicity and Metastasis through PI3K/Akt Signaling and MAPK-Dependent Focal Adhesion Disassembly. *Cancer research.* 2021; 81: 986-1000.
55. Lai I-R, Chu P-Y, Lin H-S, Liou J-Y, Jan Y-J, Lee J-C, et al. Phosphorylation of focal adhesion kinase at Tyr397 in gastric carcinomas and its clinical significance. *The American journal of pathology.* 2010; 177: 1629-37.
56. Yin K, Shang M, Dang S, Wang L, Xia Y, Cui L, et al. Netrin-1 induces the proliferation of gastric cancer cells via the ERK/MAPK signaling pathway and FAK activation *Corrigendum in/10.3892/or.* 2018.6863. *Oncology reports.* 2018; 40: 2325-33.
57. Ding Q, Gladson CL, Wu H, Hayasaka H, Olman MAJJoBC. Focal adhesion kinase (FAK)-related non-kinase inhibits myofibroblast differentiation through differential MAPK activation in a FAK-dependent manner. *Journal of Biological Chemistry.* 2008; 283: 26839-49.
58. Ruoslahti E. Fibronectin in cell adhesion and invasion. *Cancer metastasis reviews.* 1984; 3: 43-51.
59. Izumi D, Ishimoto T, Miyake K, Sugihara H, Eto K, Sawayama H, et al. CXCL12/CXCR4 activation by cancer-associated fibroblasts promotes integrin  $\beta$ 1 clustering and invasiveness in gastric cancer. *International journal of cancer.* 2016; 138: 1207-19.
60. Omland SH, Wettergren EE, Mollerup S, Asplund M, Mourier T, Hansen AJ, et al. Cancer associated fibroblasts (CAFs) are activated in cutaneous basal cell carcinoma and in the peritumoural skin. *BMC cancer.* 2017; 17: 675.
61. Tsuyada A, Chow A, Wu J, Somlo G, Chu P, Loera S, et al. CCL2 mediates cross-talk between cancer cells and stromal fibroblasts that regulates breast cancer stem cells. *Cancer research.* 2012; 72: 2768-79.
62. Nieh SJCR. The role of cancer-associated fibroblast-induced chemokine ligand 11 in tumor microenvironment contributes to the progression of oral cancer. *Cancer research.* 2017.
63. Smith HA, Kang Y. The metastasis-promoting roles of tumor-associated immune cells. *J Mol Med (Berl).* 2013; 91: 411-29.
64. Tanaka H, Yamakoshi Y, Sakimura C, Mori T, Deguchi S, Miki Y, et al. [Biomarkers for Immunotherapy Based on the Local Microenvironment of Gastric Cancer]. *Gan To Kagaku Ryoho.* 2020; 47: 1292-7.
65. Lei Y, Li X, Huang Q, Zheng X, Liu M. Progress and Challenges of Predictive Biomarkers for Immune Checkpoint Blockade. *Front Oncol.* 2021; 11: 617335.
66. Matsueda S, Graham DY. Immunotherapy in gastric cancer. *World J Gastroenterol.* 2014; 20: 1657-66.
67. Koizumi K, Hojo S, Akashi T, Yasumoto K, Saiki IJCs. Chemokine receptors in cancer metastasis and cancer cell-derived chemokines in host immune response. *Cancer science.* 2007; 98: 1652-8.

68. Le DT, Durham JN, Smith KN, Wang H, Bartlett BR, Aulakh LK, et al. Mismatch repair deficiency predicts response of solid tumors to PD-1 blockade. *Science*. 2017; 357: 409-13.
69. Le DT, Uram JN, Wang H, Bartlett BR, Kemberling H, Eyring AD, et al. PD-1 Blockade in Tumors with Mismatch-Repair Deficiency. *N Engl J Med*. 2015; 372: 2509-20.
70. Wang Z, Zhao X, Gao C, Gong J, Wang X, Gao J, et al. Plasma-based microsatellite instability detection strategy to guide immune checkpoint blockade treatment. *J Immunother Cancer*. 2020; 8.
71. Choucair K, Morand S, Stanbery L, Edelman G, Dworkin L, Nemunaitis J. TMB: a promising immune-response biomarker, and potential spearhead in advancing targeted therapy trials. *Cancer Gene Ther*. 2020; 27: 841-53.
72. Klein O, Kee D, Markman B, Carlino MS, Underhill C, Palmer J, et al. Evaluation of TMB as a predictive biomarker in patients with solid cancers treated with anti-PD-1/CTLA-4 combination immunotherapy. *Cancer Cell*. 2021; 39: 592-3.
73. Kim HR, Park HJ, Son J, Lee JG, Chung KY, Cho NH, et al. Tumor microenvironment dictates regulatory T cell phenotype: Upregulated immune checkpoints reinforce suppressive function. *J Immunother Cancer*. 2019; 7: 339.
74. Owa T, Yoshino H, Yoshimatsu K, Nagasu T. Cell cycle regulation in the G1 phase: a promising target for the development of new chemotherapeutic anticancer agents. *Curr Med Chem*. 2001; 8: 1487-503.
75. Pucci B, Kasten M, Giordano A. Cell cycle and apoptosis. *Neoplasia*. 2000; 2: 291-9.
76. Foster IJR. Cancer: A cell cycle defect. *Radiography*. 2008; 14: 144-9.
77. Wu HJ, Hao M, Yeo SK, Guan JL. FAK signaling in cancer-associated fibroblasts promotes breast cancer cell migration and metastasis by exosomal miRNAs-mediated intercellular communication. *Oncogene*. 2020; 39: 2539-49.
78. Xuefeng X, Hou M-X, Yang Z-W, Agudamu A, Wang F, Su X-L, et al. Epithelial-mesenchymal transition and metastasis of colon cancer cells induced by the FAK pathway in cancer-associated fibroblasts. *Journal of International Medical Research*. 2020; 48: 0300060520931242.